The Electronic Determinants of Spin Crossover Described by Density Functional Theory

Kasper Planeta Kepp

Abstract Spin crossover (SCO) plays a vital role in living systems and in many emerging technologies, and the accurate prediction and design of SCO systems is of high current priority. Density functional theory (DFT) is the state-of-the-art tool for this purpose due to its ability to describe large molecular electronic systems with an accuracy that can be predictive if carried out correctly. However, the SCO tendency, i.e., the free-energy balance of high- and low-spin states, is extremely sensitive to the theoretical description and physical effects such as dispersion, relativistic effects, and vibrational entropy. This chapter summarizes the recent fundamental insight into SCO gained from DFT and efforts that approach the accuracy needed (~10 kJ/mol) for rational design of SCO to become reality.

1 Introduction

Spin crossover (SCO) is the process, whereby two electronic states of different quantum-mechanical spins interconvert upon perturbation such as chemical bonding, temperature, light, or applied pressure [1–9]. Since its discovery in coordination complexes [10], it has emerged as one of the most important chemical processes [1–3, 11]. If this importance is not immediately appreciated, please consider that without SCO, the reader would suffocate within 2–3 min due to the absence of O_2 binding to hemoglobin within the honorable reader's lung arteria.

Some chemical systems can undergo transition between the two spin states without any change of chemical composition, whereas others only do so upon interaction with other molecules, such as ligand binding to a metal. The term "SCO system" or "SCO complex" is mainly used if the transition occurs relatively near standard conditions of temperature and pressure. Thus, thermal SCO systems are particularly notable as those where SCO occurs close to atmospheric pressure and within the range of room temperature by a few hundred Kelvin. Such systems are central to life

K. P. Kepp (✉)
DTU Chemistry, Technical University of Denmark, 2800 Kongens Lyngby, Denmark
e-mail: kpj@kemi.dtu.dk

E. Broclawik et al. (eds.), *Transition Metals in Coordination Environments*,
Challenges and Advances in Computational Chemistry and Physics 29,
https://doi.org/10.1007/978-3-030-11714-6_1

processes via the management of $^3O_2$ by hemes [12–14]. They are also important to many emerging technologies [1, 3], as they manifest as two distinct quantum states that can be interconverted by external stimuli. This makes them suitable for, e.g., molecular electronics [3, 15–17], sensors [18–20], and nano-mechanical behavior such as molecular motors [3, 7, 21–27].

For convenience, we will write the SCO process as a conversion from a low-spin state (LS) to a high-spin state (HS),

$$\mathrm{LS} \rightleftharpoons \mathrm{HS} \tag{1}$$

where the HS state has the highest spin quantum number or, if this number is not well-defined, the largest magnetic moment due to parallel alignment of electron spins. The fundamental requirement of SCO is then that the free energy difference of the two electronic spin states approaches zero [2, 28, 29]:

$$\Delta G_{\mathrm{SCO}} = \Delta H_{\mathrm{SCO}} - T\,\Delta S_{\mathrm{SCO}} \approx 0 \tag{2}$$

The enthalpy ΔH_{SCO} largely derives from changes in the ground-state electronic structure during SCO. These effects can be obtained from electronic energy calculations using standard quantum-mechanical programs and a suitable Hamiltonian, but it includes various energy terms not always considered that systematically contribute to ΔH_{SCO}, most notably the differential zero-point energy, dispersion forces, and relativistic effects of the two states [28, 30]. In contrast, the entropy of the process ΔS_{SCO} to a large extent (but not completely) arises from changes in the vibrational state functions [2, 30, 31] and favors the weaker and longer M–L bonds of the HS state [24, 28, 32, 33]. The electronic degeneracy contribution to this entropy is somewhat less important than the vibrational entropy of the involved chemical bonds [28, 30, 34, 35], as first recognized by Sorai and coworkers [24, 32].

Written as in (1) and (2), because ΔS_{SCO} is positive, higher temperature will favor the right-side HS state via $-T\Delta S_{\mathrm{SCO}}$ of (2), and thus conversion from an initial LS state to HS is induced by raising the temperature [24, 29]. It turns out by inspection of experimental data for iron SCO systems, but it remains to be confirmed as a general law, that the entropy and enthalpy terms of (2) tend to compensate each other substantially, as also seen in some other processes [36]. This would suggest that SCO may be a true entropy–enthalpy compensation process not just with entropy favoring reaction toward the right, but with the two terms canceling over a broad range of enthalpies and entropies; this possibility is explored further in the present chapter as it has direct implications for accurate prediction of the SCO tendency.

Transition metal ions of the middle of the first row of the d-block, specifically Mn, Fe, and Co, are particularly common in SCO systems: SCO has been observed in d^4, d^5, d^6, d^7 and arguably in some Ni(II) d^8 systems [37]. This is partly because the ligand field stabilization energy has a magnitude that makes the vibrational entropy cancel the energy terms almost perfectly. However, the balance is a compromise between the metal ion and ligand field strength, as both contribute to the SCO tendency. This is

illustrated by the spectrochemical series of the ligands and the corresponding series of the metal ions [38, 39]. Thus, for example, most SCO systems contain moderate-field nitrogen-donor ligands combined with Fe(II), as exemplified by the much studied, first synthetic iron(II) SCO system $Fe(Phen)_2SCN_2$ [40–43]. However, Fe(III) and Co(II) are also relatively common SCO metal ions, with the first-reported Fe(III) SCO systems being those of Cambi et al. [10] and the first Co(II) SCO system being that of Stoufer et al. [44].

In this chapter, the basis for describing SCO accurately by chemical–physical principles and the role of various contributions to the SCO tendency will be discussed. These include important systematic energy terms, i.e., the zero-point vibration energy, relativistic contributions to SCO, and dispersion forces that modulate the HS–LS equilibrium already at the single-molecule level. The importance of modeling the vibrational entropy contribution in the theoretical study of SCO systems is emphasized. The difference between the spectrochemical series and the "thermochemical series" of spin-state propensities are discussed. The performance of DFT and various ingredients of the functionals that affect the accuracy are analyzed.

2 Fundamentals of Spin Crossover

2.1 The Dilemma and Choice Between LS and HS

As taught in basis inorganic chemistry, when ligands are placed around a metal ion, the energies of the d-orbitals split into several energy levels due to the symmetry breaking, i.e., the d-orbitals experience different environments. If the ligand field is octahedral (O_h symmetry), two levels occur: The two high-lying degenerate e_g orbitals are aligned toward the ligands and thus experience more electronic repulsion, and the threefold degenerate low-lying t_{2g} orbital level becomes less repelled as these orbitals (originating from d_{xy}, d_{xz}, and d_{yz}) distribute further from the ligands.

Depending on the energy splitting Δ_o between the two levels, the electrons face a dilemma after occupying the three t_{2g} orbitals by one electron according to Hund's Rule: Either the additional electrons distribute in the normal fashion by pairing with the three first t_{2g} electrons or, if the energy distance is small, they may in fact move to the next level, e_g. The solution to this dilemma partly (but not completely, as discussed below) lies in resolving the relative magnitude of the penalty of moving up to the e_g orbitals, i.e., Δ_o, versus the penalty of occupying a t_{2g} orbital where another electron is already residing close in space, i.e., the spin-pairing energy penalty P. This situation is also entropically unfavorable, to be discussed below. If the fourth and fifth electron decide to move to e_g, the system will experience more aligned electron spins; this state is the HS state. If it is more favorable to pair with the t_{2g} electrons first, the resulting spin and magnetic moment becomes smaller; this is the LS state.

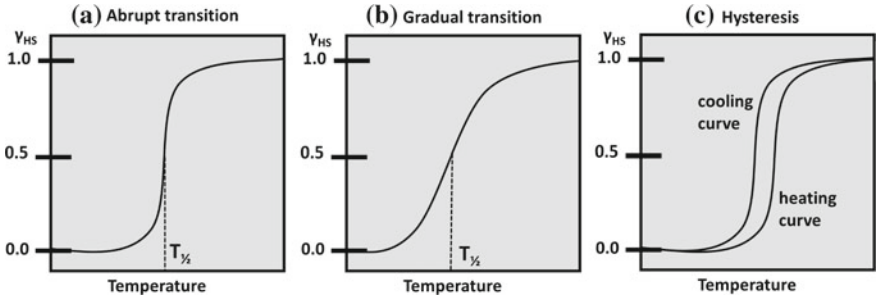

Fig. 1 Schematic representation of the transition from a low-spin electronic state with zero or little magnetism, which dominates at low temperature, to a more magnetic high-spin state, which dominates at higher temperature. **a** Abrupt transitions increase magnetism quickly near the transition temperature; **b** gradual transitions display smaller temperature gradients of the magnetism near transition; **c** hysteresis involves different transition temperatures upon heating and cooling

The question now arises: What happens if this dilemma remains unsolved, in other words, if the energy cost of pairing in the same orbitals and the entropy loss associated with this more compact LS state is almost perfectly outweighing the benefits of the lower orbital energies? If this is the case, the two possible occupations may be realized not far from standard conditions, as speculated by Pauling in his third paper in the series on the chemical bond, where he discussed the magnetic criterion for transition between HS and LS states [45]; these systems are the SCO systems.

The temperature at which the conversion in (1) takes place is referred to as the transition temperature, $T_{½}$, the temperature at which half of the system is in the HS state (the most magnetic), written as $\gamma_{HS} = ½$, and the other half is in the LS state (the least magnetic or even diamagnetic state, as in, e.g., Fe(II) LS), written as $\gamma_{LS} = ½$. Accordingly, at higher temperature, the fraction of HS, γ_{HS}, exceeds ½. This situation is shown schematically in Fig. 1a for an abrupt transition. The process can also be considerably more gradual, as shown schematically in Fig. 1b, characterized by a smaller magnetic susceptibility gradient at $T_{½}$. For abrupt processes, hysteresis is commonly observed (Fig. 1c), as discussed in detail in this chapter. At $T_{½}$, the isobaric heat capacity C_p displays a major peak reflecting the transition, being either narrow and steep or broader depending on whether the transition is abrupt or gradual [24].

Under actual equilibrium conditions, which are rarely realized in practice, the equilibrium constant K_{SCO} is equal to unity and the free energy of the process is then $\Delta G_{SCO} = 0$. However, due to the nonequilibrium nature of the actual transition, one can hardly consider this definition exact. Still it is theoretically meaningful to separate contributions to the free energy and transition temperature, as the following discussion shows. Simply put, the core premise of theoretical studies of SCO is that if the relationship holds, we should be able to predict $T_{½}$ from an estimate of $\Delta G_{SCO} = 0$, determined by electronic structure calculations. Under such conditions,

$T_{½} = \Delta H_{SCO}/\Delta S_{SCO}$, which can, as discussed below, be obtained from quantum-chemical computations at variable accuracy.

2.2 The Spectrochemical Series

In text books, the spectrochemical series [38, 46, 47] is traditionally used to estimate the preference for either HS or LS in a given coordination complex. This series is based on spectroscopic measurements of the absorption peak for the d–d transitions of cobalt(III) complexes and ranks common coordinating ligands according to Δ_o in an octahedral field. A rough rule-of-thumb order is:

$$I^- < Br^- < Cl^- < F^- < S\ \sigma\text{-donor} < O\ \sigma\text{-donor} < N\ \sigma\text{-donor} < \pi\text{-acceptors}$$

Although sometimes forgotten, this series is mainly based on Co(III), and the series, more specifically, the ligand field stabilization energy calculated from Δ_o, estimates the relative preference for HS versus LS *if this preference was only due to electronic energy* as measured by the absorption spectroscopy. The series, moreover, reflects a non-thermal electronic excitation, whereas the SCO systems of interest involve the thermal excitation of typically two electrons. Although widely used and displayed in textbooks, the estimates based on the spectrochemical series thus miss vibrational relaxation, spin pairing, and entropic effects, and they do not necessarily accurately convey the spin-state preference in a real chemical system at thermal equilibrium. Still, because the energy described by absorption maximum is a large part of the typical thermodynamic preference between the spin states, it is often accurate when applied to trend predictions, which largely explains its success [48–51].

2.3 The Thermochemical Spin Series

The real thermochemical spin-state preference and thus the adequate tool for rationalizing and predicting SCO can be argued to be a "thermochemical series" of spin-state propensity [52]. This series takes into account ground-state geometry relaxation of the HS state and entropy terms that also favor HS [31, 52, 53]. This series is straightforward achievable from DFT computations of the fully relaxed ground-state geometry of the HS state, which corrects the spectrochemical series based on electronic transitions in which the HS state features as an excited state. Furthermore, DFT can compute the vibrational entropy term with decent accuracy [36, 52, 54] so that the real preference as given by the free energy in (2) is honored. The series is importantly independent on the functional used [52], because the trend of interest involves cancellation of the major systematic errors in DFT that are discussed below.

The resulting thermochemical series resembles the spectrochemical series, but notably differs in several aspects. One of the most interesting differences is that Cl^- and Br^- have similar spin-state propensity once the thermochemical, spin-pairing, and vibrational-structural corrections are accounted for [52]. In the spectrochemical series, they separate clearly in the halide trend. Another difference is the preference for negatively charged versus neutral π-acceptors such as CN^- and CO, which change place in the thermochemical series depending on the oxidation state of the metal ion. A third difference relates to coordination isomers such as $\underline{S}CN^-$ and $\underline{N}CS^-$ that also change relative position depending on metal oxidation state [52], of relevance to the much studied SCO system $[Fe(SCN)_2(Phen)_2]$ and its derivatives.

The thermochemical series is quantitative and includes vibrational relaxation and entropy terms directly [52]. Thus, one can predict that Mn(III) systems will have relatively similar ligand preferences as Fe(II) in order to induce SCO, whereas Fe(III) should have a slightly weaker total ligand field; Co(II) SCO systems are predicted to be realized with stronger ligand fields than for Mn(III), Fe(III), and Fe(II), and even stronger ligand fields are required for Mn(II) such that even CO and CN^- become relevant. In contrast, Co(III) requries very weak ligands due to its strong LS preference, with SCO most likely occuring between F^- and weak O-donor ligands such as water, ethers, and alcohols [52]. Examples of SCO systems that illustrate these preferences are shown in Fig. 2, with 6N coordination for Fe(II) (Fig. 2a), weaker 4N2O coordination for Fe(III) (Fig. 2b), tunable ligand fields for porphyrins with Fe(II)/Fe(III) (Fig. 2c), 6N coordination for Co(II) (Fig. 2d), and correspondingly weaker 6O ligand field for Co(III) (Fig. 2e).

2.4 The Oxidation State on the Central Metal Ion

The metal ion's oxidation state plays a major role in defining the spin-state propensity, with higher oxidation state favoring LS. This effect ("the spectrochemical series of the central ions") was originally formulated by Jørgensen on the basis of spectroscopic data [39], but its fundamental truth is easily recovered and even quantified using modern DFT [52]. Specifically, a difference in LS preference of Fe(II) and Fe(III) of ~50 kJ/mol has been estimated [52]; for Co(III) versus Co(II), the difference is even higher and can reach 100 kJ/mol [52]. This effect clearly needs to be considered if SCO systems of variable metal oxidation states are to be developed by rational screening.

The fact that Fe(III) favors LS more than Fe(II) is easily understood from the stronger and shorter metal–ligand bonds formed in the higher oxidation states, which increases the σ-donation and thus the ligand field splitting and tendency toward low spin. Because of this, the most common coordination structure for Fe(II) SCO systems is 6N [55], whereas for Fe(III) SCO systems, the 4N2O coordination structure is common [6], where two nitrogen donors have been changed into weaker oxygen donor atoms. There are many exceptions to this preference: For example, some 4N2O iron(II) systems have been reported [56], and an Fe(II) 5N1S system has been made

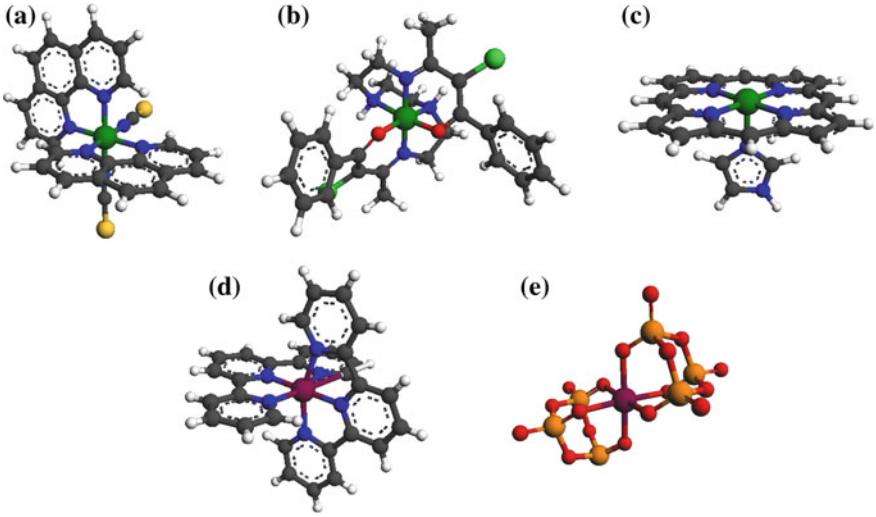

Fig. 2 Some examples of mononuclear SCO coordination complexes: **a** the iron(II) compound $[Fe(SCN)_2(Phen)_2]$; **b** the iron(III) compound $[Fe(bzacCl)_2trien]^+$ (bzac = benzoylacetonate-triethylenetetramine); **c** deoxyiron(II)porphine as a generalized representation of porphyrins and hemes; **d** the cobalt(II) compound $[Co(terpy)_2]^{2+}$; **e** the cobalt(III) compound $[Co(P_3O_9)_2]^{3-}$

[57]. This is possible because the constraints imposed by the thermochemical spin preference of the monodentate ligands can be broken in more complex coordination environments where the σ-donation is modulated electronically either by induction effects to the donor atom or by strained geometries, as commonly seen in SCO systems using multidentate ligands.

2.5 Homoleptic SCO Complexes and the Case of $Co^{3+}(aq)$

Very few, if any, real SCO systems possess O_h symmetry (one candidate is $[NiF_6]^{3-}$). Even if the complex is homoleptic (sharing chemically identical ligand donor atoms) as is reported in few cases [58, 59], Jahn–Teller distortion will cause the t_{2g} and e_g levels to split for the d^4 HS and LS configurations, for the d^6 HS configuration, and for the d^5 and d^7 LS configurations. Thus, the O_h symmetry is broken in almost all real cases to a variable extent. In fact, it would be an interesting academic challenge to identify a homoleptic SCO system that possesses almost perfect, unstrained O_h symmetry without Jahn–Teller distortion in one of its spin states, i.e., d^5 HS or d^6 LS. This state would represent an intrinsic, unstrained fit of the ligand and metal to enable SCO, something that puts major restriction on the exact ligand fields' strength of the six identical donor atoms.

Homoleptic coordination complexes for a range of different simple monodentate ligands with these d-electron configurations for Mn(II), Mn(III), Fe(II), Fe(III), Co(II) and Co(III) have been studied by DFT [52] and can help to suggest how such an "ideal" symmetric homoleptic system may be realized. Using the functionals known to be more accurate for the purpose (e.g., B3LYP* [60, 61] or TPSSh [62], e.g., as shown previously [63, 64]), one sees that some combinations of metal ions and ligands can bring a homoleptic complex very close to SCO. Co(III) has the strongest LS preference of all first-row d-block metal ions up to the III oxidation state as it has maximal ligand field stabilization energy in LS due to its t_{2g}^6 configuration and has higher charge than the iso-electronic Fe(II) LS. Thus, Co(III) SCO systems are rare and require very weak total ligand field strengths to reach SCO; the 6O coordination structures by Kläui and associates are notable in this regard [65–67]. Examples of Co(III) SCO may also exist in mixed-metal oxides [68], and a new example of a bistrimetaphosphate Co(III) complex with probable SCO properties was reported recently (Fig. 2e) [69]. In contrast, Co(II) SCO systems are relatively common and often feature 6N-coordination structures, e.g., bis-terpyridines (Fig. 2d) [70], consistent with the discussion above [71–73].

This raises an interesting and important question, namely how far above the LS state is the HS state of Co(III)(aq)? All other M(aq) systems of the first row of the d-block are HS due to water's weak ligand field, and their spin states were recently studied by CASPT2 [74]. Standing out alone, Co(III) is known to be LS under typical conditions studied (which are very acidic, because Co(III)(aq) readily undergoes reductive hydrolysis to Co(II) at neutral pH). Moreover, $[CoF_6]^{3-}$ is known to be HS, and this makes the range to HS very small since H_2O is close-by in the spectrochemical series [38]. The Co(III)(aq) is assumed (and has been shown in older data) to feature LS, but this produces several anomalies such as a much faster self-exchange electron transfer rate and faster ligand substitution than expected. Recent DFT computations [75] of the relative self-exchange rates of hydrated transition metal ions accurately recover the experimental 10^5 anomaly of Co(II)/Co(III) when plotting the trend in reorganization energies versus experimental rate constants and using LS Co(III) as commonly assumed. When doing the same correlation for HS Co(III)(aq), the anomaly disappears almost completely. DFT can also be used to correct previous spectroscopic estimates of the HS–LS gap with entropy and vibrational geometry relaxation showing that Co(III)(aq) is very close to SCO. In conclusion, this analysis converges on the view that the HS state is probably active during much of the chemistry of the hydrated Co(III), in stark contrast to text book consensus based on early NMR and absorption spectroscopy measurements in strong acid [76–78], but explaining the anomalous high ligand substitution and electron transfer capabilities of Co(III)(aq) [79, 80]. Indeed, several SCO systems of Co(III) with O-donor ligands are known [66, 68]. Future exploration of the SCO properties of Co(III) in water-like coordination environments should therefore be of interest.

2.6 Geometry Preferences and Changes During SCO

In the HS state, e_g occupation and associated ligand d-electron repulsion expands the metal–ligand bond lengths [52, 81]. Accordingly, LS states are generally more compact than HS states, and the system tends to expand upon SCO to the HS state [2], as schematically shown in Fig. 3a. However, despite the increased molar volume, the crystal symmetry is typically unaffected [24]. The longer, weaker, and more entropic metal–ligand bonds largely explain why HS is favored by temperature, viz the $T\Delta S$ term in (2). It is also the main reason why applied pressure tends to often favor the more compact LS state. In a crystal state, expansion of the core system leads to a larger unit cell and to a change in the intermolecular crystal packing forces. In a solution state, the expansion can affect the solvation energy of the two states differently, since the HS state will tend to be a slightly larger solute [28]. Not only the bond lengths but also the bite angles and the distances between the N-donor atoms of multidentate ligands may change accordingly, and the different geometric preferences of the two electronic states can thus sometimes be used to predict spin-state preferences by simple geometric inspections [58].

To put approximate numbers to this geometry effect, one can again turn to systematic studies of homoleptic mononuclear octahedral coordination complexes [52]. A summary of this analysis is shown in Fig. 3b. It turns out that the geometry changes upon the conversion of spin state are very dependent on the involved ligands and metal ion. Importantly, the geometry change scales almost monotonically with the ligand field strength such that weak-field halides give small geometry changes of the order of 0.02–0.12 Å (depending on metal ion), whereas larger changes of 0.15–0.40 Å occur for strong-field π-acceptor ligands [52]. Furthermore, the *variation* in geometry relaxation also scales with ligand field strength. This implies that the metal ion effect on HS–LS geometric relaxation upon SCO is much larger for strong-field

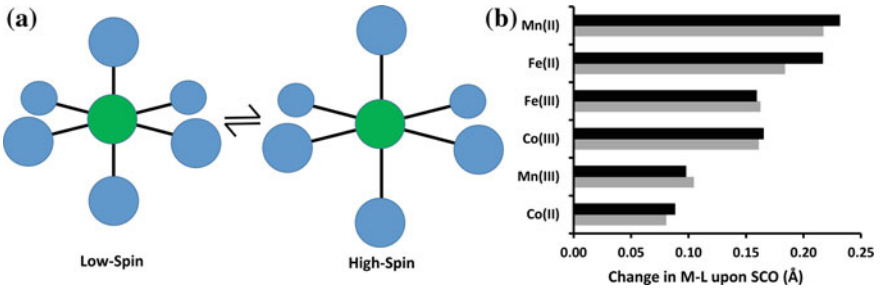

Fig. 3 **a** Schematic representation of the change in geometry associated with a transition from a LS state to a HS state in a mononuclear coordination complex; **b** DFT-computed changes in average metal–ligand bond lengths for d^4–d^7 configuration systems. The present figure is made from previously published data [52]: black color shows results for hexamine complexes, whereas gray color shows the average over a range of ligand types (halides, O-, and N-donor, and strong π-acceptors)

ligands than for weak-field ligands. The largest structural effects are, interestingly, seen for Mn(II) and Fe(II). A change of 0.2 Å or 0.3 Å is considerable; it occurs on average for all six bonds in a six-coordinate complex. For Fe(II) SCO systems with N-donor ligands, one can expect a typical average increase in Fe–N bond length of ~0.2 Å, as shown in black color for Fe(II) in Fig. 3b [52].

As discussed below, metal ions with large structural relaxation upon SCO are expected to also show more abrupt transitions with hysteresis. Accordingly, DFT as summarized in Fig. 3b largely explains why Fe(II) SCO systems commonly display high hysteresis but also predicts that Mn(II) systems should have similar or even larger ability to do so, of course under a modulating influence of other effects outside the first coordination sphere.

Since the geometric and environmental effects required to cause SCO can be subtle, SCO may be induced by adsorption of one molecular system to another, as the adsorbed state affects the molecular environment of the SCO system. The classic example is the host–guest systems [82], such as that of Halder and Kepert et al. [83] Supramolecular cages with SCO properties constitute one class of systems [84], whereas a recent example of "on-surface" SCO is that of Kumar et al. [85] Hemes, which are well known to change spin state upon changes in coordination environment, also seem to undergo on-surface SCO upon relatively weak adsorption to, e.g., gold surfaces [86], although this finding needs stronger experimental bearing.

2.7 The Nature of the SCO Transition

The actual transition from one spin state to the other can occur either gradually, or abruptly, and be subject to small or large hysteresis, as shown in Fig. 1. It is also possible, although not shown in Fig. 1, to have a multistep transition, and two-step processes have recently been studied by DFT [27]. Such multistep processes typically arise from a heterogeneous SCO sample, i.e., the presence of two or more the individual and distinct sites undergoing SCO, or possibly from restructuring of the system (including solvent) near the transition temperature.

The SCO transition curve has a sigmoidal form characteristic of a cooperative process. The cooperativity can be partly due to magnetic alignment as seen in an Ising model, and partly to structural phase transitions occurring locally: If the molecules interact closely, the intermolecular interactions produce free energy minima distinct to the larger HS and smaller LS volume. Accordingly, the conversion into a given spin state of one molecule makes it more favorable for neighbor molecules to attain the same spin state [27]. The extent of cooperativity, and accordingly the abruptness of the transition, thus depends greatly on the surroundings of the single molecule. In a solid, each magnetic center has contact with several neighbors, and thus the geometric spin-state preference induces a friction in the tendency to change spin state, which is greatly influenced by intermolecular interactions. In a solvent, cooperative interactions can be modulated by the presence of counter ions and solvent molecules, and the solvent can separate the SCO solutes so well that the spin transition becomes

gradual. Accordingly, the transition behavior is typically very different in solid and solution [2, 3], and largely influenced by electrostatic interactions of molecules [87]. Covalent linkers and hydrogen bonds can be introduced to enhance the cooperativity [2, 3, 25, 88].

Hysteresis, defined as magnetization curves that differ upon heating and cooling *for the same molecular composition*, is shown schematically in Fig. 1c. Hysteresis is a priori expected during SCO because of the change in molar volume associated with the more expanded HS state. In case of hysteresis, one has to distinguish two transition temperatures, $T_{½}$ (↑) for heating and $T_{½}$ (↓) for cooling. Because of the "friction" due to the distinct cooperative interactions in each state of distinct molar volumes, it generally holds that $T_{½}$ (↓) < $T_{½}$ (↑) (Fig. 1c). The difference in these two values,

$$\Delta T_{½} = T_{½}(\uparrow) - T_{½}(\downarrow) \tag{3}$$

defines the extend of hysteresis. For the purpose of theoretical modeling, the *single* molecule $T_{½}$ can be assumed to be

$$T_{½} \approx \left(T_{½}(\uparrow) + T_{½}(\downarrow) \right) / 2 \tag{4}$$

The *intermolecular* correlations causing $\Delta T_{½}$ should then be modeled separately [89]. Hysteresis may be utilized technologically because it produces a molecular "memory" to the system near the transition region [88]. Accordingly, large hysteresis is rare but desired for the purpose of switchable materials [4, 90].

2.8 True Hysteresis and Intrinsic Hysteresis

True hysteresis is defined only for systems where the composition is identical before and after transition. However, many SCO systems are prepared as hydrates, or with other co-crystallized molecules. Many transitions of interest occur at temperatures where these molecules begin to evaporate from the complexes, and this process is irreversible. Accordingly, if $T_{½}$ provides thermal energy enough to release these molecules, a large separation in the first heating and subsequent cooling curves will be observed which is *not* hysteresis, but simply reflects two different molecular systems being studied. Thus, several of the SCO systems reported to have large hysteresis may in fact reflect different molecular systems rather than true hysteresis [24]. Any technological application of hysteresis obviously requires microscopic reversibility, which is only obtained with stable systems of the same composition. This requirement substantially narrows down the number of observed cases of very large "true" hysteresis.

Inspection of $\Delta T_{½}$ values suggests a natural or *intrinsic* hysteresis of 0–20 K for many studied cases, which for some SCO systems is augmented by additional hysteresis. Although not discussed there, this can be inferred from the data compiled

by Sorai [24]. The intrinsic hysteresis probably reflects the simple volume reordering effects of the first coordination sphere, which is approximately similar for all SCO systems (although the expansion depends on ligand and metal type as discussed above). Additional contributions to $\Delta T_{½}$ can arise from larger reorganizations due to bulky groups or intermolecular interactions beyond the local volume changes of the first coordination sphere that is generic to all SCO systems; this distinction between two parts of the hysteresis (which is, as a disclaimer, only the author's view) probably warrants further exploration.

As shown in Fig. 3b, Fe(II) systems exhibit some of the largest geometric changes upon SCO among d^4–d^7 systems [52]. Consistent with the volume-friction interpretation discussed above, this probably explains why Fe(II) more commonly displays hysteresis in comparison with other SCO systems [2]. This observation seems to confirm that hysteresis at least partly arises from the geometric friction of the heating and cooling processes caused by the different free energy minima at different molar volumes for HS and LS. The intermolecular interactions that define the transition are diverse and harder to systematize than the electronic structure of the molecule itself, but the intrinsic contribution from the first coordination sphere, as discussed above, seems to be predictable by DFT, which computes geometric changes with good accuracy.

3 Important Contributions to Single-Molecule SCO

3.1 Zero-Point Vibrational Energy

The vibrational zero-point energy (ZPE) is one of the electronic effects that always contribute to the SCO tendency regardless of the environment. It has been known for a long time, and was described clearly in the pioneering DFT work on SCO by Paulsen et al. [34], that the differential ZPE of the HS and LS states is an important contribution to the SCO process. This paper also reported the strong bias toward LS of the non-hybrid GGA functionals and the preference for HS for the hybrid B3LYP functional, an important observation that, for example, motivated the later development of the B3LYP* functional by Reiher et al. with a smaller 15% HF exchange [60].

The importance of ZPE lies both in the fact that its magnitude is of the order of 10 kJ/mol [34, 64], similar to the typical values of the full ΔH_{SCO} [36], and it is systematic, as it almost exclusively favors the HS state. This favoring follows directly from the longer and weaker M–L bonds of the HS state, which accordingly have smaller ZPEs than the LS states. Not only the SCO process but also a general chemical process involving multiple spin states will experience this effect. On an energy profile of competing spin states, neglect of ZPE will tend to provide an artificial bias in favor of the LS states in the reaction coordinate diagram.

More systematic studies of the ZPE contribution indicate that the differential ZPE is very dependent on the type ligand and to a lesser extent the type of metal ion [52]: Typical differential ZPEs in favor of HS range from 5 to 25 kJ/mol and grow more or less monotonically with the ligand field strength. Accordingly, for weak ligands such as halides, the differential ZPE can be almost neglected, whereas for strong-field π-acceptor ligands such as CN^- and CO, the ZPE dramatically favors HS by more than 20 kJ/mol. Thus, the importance of remembering the ZPE correction depends very much on the system of interest. This follows trivially from the fact that the ZPE scales monotonically with the overall strength of the M–L bond, which again scales with the ligand field strength. In the middle range, typical ligands relevant to SCO systems have differential ZPEs of 10–15 kJ/mol [52]. The ZPE can also vary by >10 kJ/mol due to metal ion and d^q configuration. This also affects the bond strengths of the M–L bonds in the two spin states, but since these d^q configurations vary substantially in terms of electronic structure and some, such as HS Mn(III) and LS Co(II) induce strong Jahn–Teller distortions, this metal effect is not trivial to interpret.

3.2 Dispersion Contributions to the Spin Crossover Equilibrium

Dispersion effects are the second-order interaction of instantaneously induced dipole moments of electron densities that affect bonding in all systems. Dispersion is not intrinsically included in most modern density functionals, and the most popular way to do so is by using an empirically parameterized correction to the electronic energies computed by the functional, such as the popular D3 correction by Grimme and coworkers [91]. Within the last decade, dispersion corrections have become increasingly mandatory in DFT calculations of chemical structure and reactivity.

Since the dispersion forces contribute substantially to the intermolecular interactions, their inclusion is important if one wants to understand the transition behavior [92, 93]. Dispersion interactions also affect $T_{½}$ itself, by favoring either HS or LS. Depending on the nature of the ligands and their packing, dispersion forces will either compress or expand the first coordination sphere, shifting the potential energy surface either toward longer M–L bonds to favor HS or to shorter M–L bonds favoring LS. The favoring of HS or LS may be very dependent on the intermolecular ligand–ligand interactions.

A priori, dispersion effects might not be expected to contribute to the SCO tendency of *single* molecules in solution with simple monodentate ligands having no systematic steric strain. Dispersion would be expected to mainly affect closely interacting parts of different molecules, or bulky parts of the same molecule. With the advent of empirical dispersion corrections of DFT, one could explore whether dispersion forces also contribute to this important process *even* at the single-molecule level, i.e., if there is a generic first coordination sphere contribution from dispersion

to the SCO thermodynamics. This question can be directly addressed by dispersion-corrected DFT [91], because the dispersion energy correction is calculated explicitly and is separated from the remaining electronic energy of the system [54].

Strained five-coordinate iron(III)porphyrins with variable substituted axial ligands have been studied with and without dispersion forces included [54]. It was found that dispersion forces contribute already for the single molecule by affecting the free energy gap of (2) by often 10 kJ/mol or more. Considering that the total ΔH_{SCO} is in the order of 5–20 kJ/mol, this makes account of the dispersion forces critical. Four of the porphines had axial phenyl ligands attached directly by Fe–C bonds with 3–5 fluorides as phenyl substituents. This produces unusual short-range interactions and clashes between the fluorine and hydrogen atoms and the porphyrin ring in these particular systems.

However, with the advent of computational dispersion corrections to DFT, it was discovered that also in most other, unstrained single molecules, intramolecular dispersion tends to favor LS due to the stronger electronic stabilization of the more compact LS state [52]. This suggests that there is a generic, intrinsic contribution of dispersion interactions to the SCO tendency arising for the first coordination sphere of any complex of typically 5–15 kJ/mol which contributes to the real, observed $T_{½}$ [36, 52]. This contribution may then be compensated or increased by other ligand–ligand interactions. In bulky systems with ligand–ligand strain from close contacts, which tend to expand the first coordination sphere and favor HS, dispersion will further remedy some of the strain and reduce the expansion, and thus by itself favor LS.

This discovery of a generic first coordination sphere dispersion contribution to SCO arises because the attractive close-range dispersion energy favors the more compact LS state more than the HS state. As an example of consequence, if dispersion is included in B3LYP (as in B3LYP-D3), the SCO prediction becomes better because the intrinsic first coordination sphere contribution to SCO is included and counteracts the HS bias, and thus B3LYP-D3 is generally more accurate than B3LYP [36, 94].

It has now been found repeatedly that the dispersion forces of the SCO process work to favor the LS state of the single-molecule first coordination sphere [36, 95, 96]. The effect can easily reach 15–20 kJ/mol and averages 10 kJ/mol for the 30SCOFE database [36]. Thus, in order to model and predict the relative thermodynamics, SCO tendency, and $T_{½}$ of a series of compounds, dispersion forces need to be explicitly included.

3.3 Relativistic Stabilization of LS

Most studies of first-row transition metal systems do not include relativistic contributions to the energy. This is probably because relativistic effects are relatively less important for Sc–Zn, and partly because relativistic computations can be very demanding in terms of computational resources. However, relativistic effects can be substantial already for the first row of the d-transition series [97], and, e.g., for

M–L bond enthalpies, relativistic effects typically surpass 5 kJ/mol [98]. It is of fundamental scientific interest to understand whether relativistic effects contribute to SCO. Also, from the point of view of theoretical prediction of SCO systems, comparing nonrelativistic energy estimates directly to the experimental energy gaps could cause an error in the conclusion on the quality of the applied nonrelativistic method, whether it be CASPT2, CCSD(T), or DFT.

It has been shown [36] that scalar-relativistic corrections to the HS–LS energy gap accurately reproduce relativistic effects computed using both second- and fourth-order Douglas–Kroll–Hess energies [99], which simplify the Dirac equation by separating the positive and negative energy states [100]. The success of scalar-relativistic estimates arises from the small spin-orbit coupling of the light transition metal ions (Mn, Fe, Co) that undergo SCO (~1 kJ/mol [101]), although spin-orbit coupling is formally required for transition to occur in the first place and plays a qualitative role in the process as seen, e.g., for light-induced SCO [102]. The Douglas–Kroll–Hess two-component formalism with and without spin-orbit coupling only changes the scalar-relativistic energies by typically ~1 kJ/mol. Order 4 and 2 give similar results within ~1 kJ/mol, and the spin-orbit coupling corrections are 0–3 kJ/mol for the HS–LS gap, justifying the use of scalar-relativistic corrections which can recover most of the real relativistic LS stabilization by fast computation [36].

It turns out that there are significant relativistic contributions to SCO [36, 103, 104]. Interestingly, the relativistic energies tend to generally favor the LS state and are quite systematic and not very variable, because they tend to be localized to the metal center rather than other lighter atoms of the SCO system. The simplest explanation for this relativistic SCO effect is that the LS state is more compact with lower spin and angular momentum, and thus features stronger stabilization (reduction in inter-shell electron repulsion) once the 1s-orbital on iron is relativistic stabilized and contracted. In contrast, the reduced effective nuclear charge resulting from relativistic contraction mainly destabilizes the diffuse higher-angular momentum d-orbitals, in particular, the e_g-type d-orbitals of the HS state [36]. This explanation of the relativistic SCO effect follows closely the standard principles seen for other observables as outlined and discussed by Pyykkö [105].

The relativistic LS stabilization averages to 9 kJ/mol for iron SCO systems [36]. This is, remarkably, of the same magnitude as the dispersion and ZPE corrections. In other words, ZPE, dispersion, and relativistic effects work together to affect the energy difference between the HS and LS states, which is of a net magnitude of 5–20 kJ/mol, and they all are of similar importance, on average ~10 kJ/mol or so [36]. These three energy terms are systematic, i.e., they tend to favor one spin state consistently. Accordingly, they need to be included if one strives toward quantitative accuracy. To summarize this important conclusion, Fig. 4 displays the impact on a hypothetical transition curve of the three energetic contributions discussed above, i.e., ZPE (Fig. 4a), relativistic stabilization of LS (Fig. 4b), and the single-molecule component of the dispersion forces (Fig. 4c). The systematic behavior of these terms may aid us in the future rational design of powerful SCO systems with the exact energy terms desired to contribute to ΔH_{SCO} of (2).

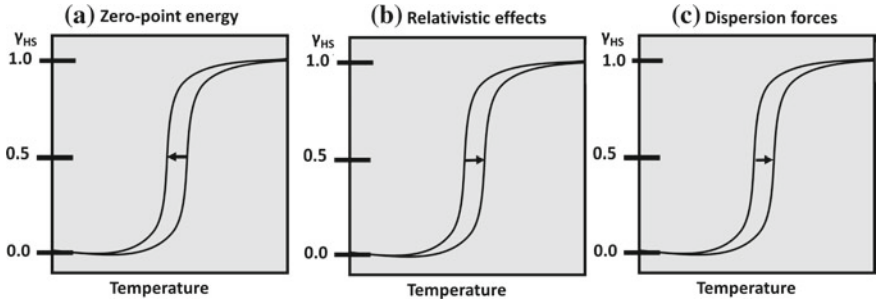

Fig. 4 Schematic representation of the theoretically expected typical impact of **a** zero-point vibrational energy, **b** relativistic effects, and **c** single-molecule dispersion forces on the transition temperature $T_{½}$, with all intermolecular effects ignored

3.4 Vibrational Entropy

The previous three sections discussed three physical effects that contribute to the energy of SCO, as measured by ΔH_{SCO}. With these three corrections to the electronic energy computed by a quantum-chemical method, one can obtain a decent estimate of how well the method performs in comparison with the experimental enthalpy of SCO. However, in order to understand and rationally predict SCO, and in particular the actual transition temperature $T_{½}$, one needs to account for the entropy term, $T\Delta S_{SCO}$ of (2), which is largely responsible for the transition to HS as the temperature is increased [24, 32, 106]. As mentioned above, the HS state contains more entropy in its longer and weaker metal–ligand bonds, due to the occupation of the e_g-type orbitals, and is accordingly favored by higher temperature because this entropy scales with T.

Paulsen et al. [34] first included vibrational entropy in the computational estimate of SCO tendency. The entropy change during SCO arises partly from the increased electronic partition function from the additional occupied orbitals (the electron configurational entropy), which provides a few kJ/mol of $T\Delta S$ in favor of the HS state near room temperature, and the vibrational entropy arising from changes in molecular geometry, which accounts for most (typically, 2/3–3/4) of the total entropy effect [24, 107]. In essentially all real SCO systems, symmetry breaks down to C_1, and the electronic degeneracy factor is no longer exactly applicable. Still the larger density of close-lying configurations prevails in the HS state and a simple estimate of the electronic degeneracy factor such as $\Delta S \sim k_B \ln \Omega$ from the Boltzmann formula gives an approximate idea of this contribution.

While Sorai and coworkers showed the importance of vibrational entropy in driving SCO [32, 107], the importance goes further: Correlation of experimental data for iron SCO systems [36] suggests that for the single-molecule first coordination sphere, the magnitude of this entropy directly relates to the enthalpy of the process, with entropy–enthalpy compensation across the range of ΔH_{SCO} and ΔS_{SCO} values for quite diverse ligand systems. Whether this is a general law remains to be

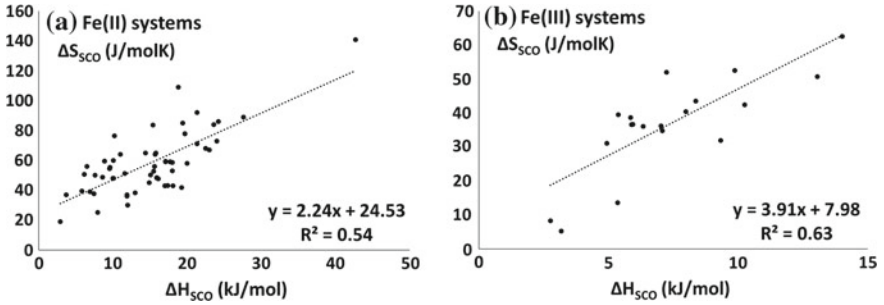

Fig. 5 Evidence for entropy–enthalpy compensation during SCO: **a** For Fe(II) systems (data were compiled from Toftlund [29], Chum et al. [109], Letard et al. [110], Strauss et al. [111], Sorai [107], Kulshreshtha et al. [35], Boča et al. [112], Nakamoto et al. [106, 113], Bartel et al. [114], and Lemercier et al. [115]); **b** for Fe(III) systems (data were compiled from Sorai [107] and Dose et al. [116])

established. However, for the purpose of this chapter, the author collected additional experimental data for ΔH_{SCO} and ΔS_{SCO} from the literature. Figure 5a shows the plot of ΔH_{SCO} and ΔS_{SCO} for a compiled data set of 62 iron(II) systems, and Fig. 5b shows this for 20 iron(III) systems for which data are available in the literature. For iron(II) systems, one set of values for $[Fe(bzimpy)_2]^{2+}$ is particular high [108] (bzimpy = 2,6-bis(benzimidazol-2′-yl)pyridine). This data point should probably be deemphasized. If correct, it doubles the range of possible ΔH_{SCO} and ΔS_{SCO} values which would be interesting. Even without this outlier, the correlation coefficient R^2 is 0.39 and remains highly significant. Figure 5 clearly shows evidence of very strong entropy–enthalpy compensation across both iron(II) and iron(III) systems during SCO and thus confirms the previous discovery [36]. Thus, not only does entropy drive thermal SCO as discovered by Sorai and coworkers [24, 32], *it also does so in proportion to the enthalpy of the same process*.

The entropy–enthalpy compensation of SCO needs to be considered when actively searching for new SCO systems and understanding their behavior. For example, an applied increased ligand field strength that increases the enthalpy of SCO in favor of LS will remarkably also tend to increase the entropy of the corresponding HS state to largely counteract the effect intended by the scientist. This compensation effect will obviously complicate rational design unless the effects are clearly separated. Understanding when the entropy–enthalpy compensation of SCO can be circumvented will thus be of particular interest.

The compensation effect also has implications for studies that estimate SCO tendency purely based on energies or proxies thereof, as has been and is still relatively common [117–119]. Most importantly, one cannot predict the $T_{½}$ or other real conditions of SCO without including the entropy because it largely counteracts the energy terms derived from standard electronic structure computations. Neglect of entropy is relatively common in studies of transition metal catalysis, metalloenzymes, and organometallic chemistry. Many systems have intermediates with close-lying spin

states that often play an important role in the chemical process [13, 120, 121]. It makes a substantial difference if one does not include a systematic effect that favors one of these spin states consistently. Examples include hydrogenases and heme proteins, where the spin states are close in energy and important for the mechanism [14, 95, 121]. The HS state is generally more entropic than the LS state, and one can expect errors of 10–20 kJ/mol [36] *per metal site* systematically underestimating the importance of the HS state if entropy is neglected. Neglect of vibrational entropy can lead to the erroneous assignment of a LS state as the ground state. Similar errors will occur in estimates of the best theoretical method based on comparing energies without entropy directly to experimental spin states, which always represent free energies that include the entropy effect.

The question then arises whether one can model this vibrational entropy with decent accuracy. Standard approaches involve the computation of the harmonic vibration frequencies of the molecule, which is already required to obtain the ZPE, which, incidentally, also favors the HS state's longer and weaker bonds. Once this calculation has been carried out, it is straightforward to estimate the vibrational entropy by using thermodynamic state functions and the calculation of the vibration partition function Q_{vib}. Most quantum-chemistry programs can routinely perform this computation. For single molecules, the vibrational entropies correlate decently with experimental ΔS_{SCO} with errors translating into typically 5 kJ/mol for $T\Delta S_{\mathrm{SCO}}$, partly because the electronic configurational entropy is relatively similar for the systems [36]. The estimates neglect differential entropy contributions from solvent–solute and crystal packing, i.e., they represent only the contribution from single SCO molecules. In terms of intermolecular contributions, both high-frequency and low-frequency modes contribute to the entropy [122–124]. One can expect the soft vibrational modes to be associated with large *relative* errors for the computed estimates. However, importantly, the high-frequency (M–L stretch) frequencies of the first coordination sphere of the single molecule dominates the entropy effect as shown by Raman spectroscopy [122], and these are well modeled by DFT [36, 92, 125]. Thus including entropy estimates for the first coordination sphere is much better than omitting them, as they improve the $\Delta G_{\mathrm{SCO}}(T)$ and thus $T_{½}$ substantially. However, given the current limitations in the accuracy of these calculations, simply adding a constant contribution of $T\Delta S$ [52] may be a reasonable approach for many transition metal systems.

The entropy contribution to the balance between the spin states depends greatly on the nature of the ligand and the metal ion, with stronger ligands showing much larger entropy effects than weak ligands [52]. Typical $T\Delta S$ contributions of 5–30 kJ/mol are estimated for mononuclear complexes at room temperature [52]. This range is similar to the experimental range seen for Fe(II) and Fe(III) SCO systems [36]. The small effects are typical of weak field or weakly bound ligands. For nitrogen-donor ligands as are commonly found in SCO systems, the entropy contribution ranges typically from 10 to 25 kJ/mol [36, 52]. The entropy contribution is relatively insensitive to the theoretical method used as long as the geometry and vibrational frequencies are reasonable. This makes the entropy contribution more straightforward to estimate than the electronic energy contribution, which is discussed in more detail below.

4 Performance of DFT for Describing SCO

4.1 The Massive Role of HF Exchange Favoring HS

In order to fully understand and predict SCO tendencies of molecular systems, the various systematic effects discussed above need to be considered and added to the electronic energy of the HS and LS states. The enthalpy of the process can be written as:

$$\Delta H_{\mathrm{SCO}} = \Delta E_{\mathrm{SCO}} + \Delta \mathrm{PV}_{\mathrm{SCO}} \tag{5}$$

The last term is small (of the order of RT) for thermal SCO, and the energy term is:

$$\Delta E_{\mathrm{SCO}} = \Delta E_{\mathrm{el,SCO}} + \Delta E_{\mathrm{rel,SCO}} + \Delta E_{\mathrm{ZPE,SCO}} + \Delta E_{\mathrm{disp,SCO}} \tag{6}$$

where $\Delta E_{\mathrm{el,SCO}} = E_{\mathrm{el}}(\mathrm{HS}) - E_{\mathrm{el}}(\mathrm{LS})$ is the direct nonrelativistic energy gap of the HS and LS states computed by a density functional without dispersion included, $\Delta E_{\mathrm{rel,SCO}} = E_{\mathrm{rel}}(\mathrm{HS}) - E_{\mathrm{rel}}(\mathrm{LS})$ is the relativistic contribution to the HS–LS energy gap (typically 5–10 kJ/mol in favor of LS and very constant), $\Delta E_{\mathrm{ZPE,SCO}}$ is the differential ZPE (typically 10 kJ/mol in favor of HS for SCO systems but very dependent on metal and ligand type), and $\Delta E_{\mathrm{disp,SCO}}$ is the differential dispersion effect on SCO (typically 10 kJ/mol in favor of LS for single molecules, but augmented with a variable contribution depending on intermolecular interactions). Commonly, these three terms sum up to a correction of 0–20 kJ/mol in favor of LS. Once the systematic effects of (5) are accounted for, it enables us to estimate the accuracy of a theoretical method toward SCO and to identify truly spin-state-balanced density functionals.

However, it turns out that the electronic Hamiltonian used to obtain the electronic energies of the states, $E_{\mathrm{el}}(\mathrm{HS})$ and $E_{\mathrm{el}}(\mathrm{LS})$ of (6), is a major problem in itself. In the world of DFT, there are hundreds of functionals with distinct acronyms to choose from, and this diversity can easily overwhelm young researchers unless their supervisors have very strong adherence to certain functionals. So which density functionals produce accurate $\Delta E_{\mathrm{el,SCO}}$?

The use of hybrid functionals, in particular B3LYP [126–128], greatly improved the accuracy of computational main-group chemistry and have accordingly also been widely applied to study inorganic chemistry. Paulsen et al. computed the energy gap between HS and LS states for nine iron complexes using B3LYP and for some of them also the non-hybrid GGA functionals PW91 and BLYP [34]. They observed that the non-hybrid functionals produce energies much in favor of LS (by up to 104 kJ/mol for PW91), whereas B3LYP favors HS. This observation that the 20% HF exchange hybrid B3LYP favors HS and that 0% HF exchange favors LS probably inspired the development of the B3LYP* functional by Reiher a year later [60, 129].

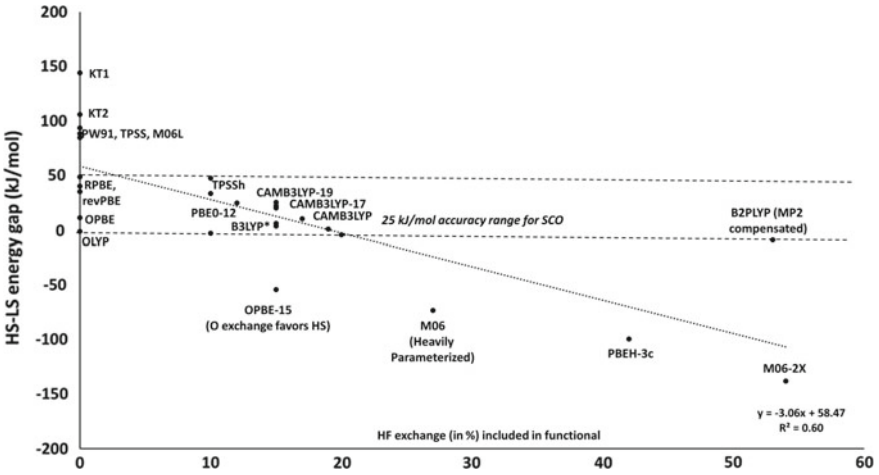

Fig. 6 The performance of various density functionals for modeling the average HS–LS energy gap of Fe(II) and Fe(III) SCO systems. The dashed line reflects a generous estimate of an acceptable result within 25 ± 25 kJ/mol of the fully corrected HS–LS gap. The figure was made using data previously published [94]

Since then it has consistently emerged that non-hybrid functionals are commonly (but with notable exceptions) not capable of describing $\Delta E_{\mathrm{el,SCO}}$ of (6) accurately [64, 89, 130–132], i.e., some inclusion of HF exchange is needed in a hybrid as is also the experience for main-group thermochemistry [133–135]. The HF state represents an artificial situation where the spin-aligned electrons are completely correlated by exchange, but the electrons of opposite spins are not correlated at all. HF exchange selectively favors HS because the exchange integrals of the Kohn–Sham determinant explicitly count only the parallel-spin electron interactions, which are more abundant in the HS state, and this exchange energy is always favorable [28, 136].

The amount of HF exchange is accordingly the single most important feature affecting $\Delta E_{\mathrm{el,SCO}}$ of a hybrid GGA functional, and $\Delta E_{\mathrm{el,SCO}}$ increases linearly with the included HF exchange [60, 61, 129, 131]. The effect depends very much on the bonding character of the t_{2g} orbitals, as recently analyzed [137]. A benchmark [36] accounting for the systematic effects of (6) concluded that B3LYP* remains one of the most accurate functionals even in competition with newer and more advanced functionals. B2PLYP [138] and TPSSh [62] also performed well. Many functionals can be tuned to perform well for SCO if they are made into hybrids with 10–20% HF exchange, suggesting that this range is perhaps generic among standard GGA functionals [94]. However, some functionals break this rule for special reasons and it is instructive to understand why this occurs. To understand these other underlying determinants of the HS–LS energy difference in more detail, the HS–LS gap for different functionals is shown in Fig. 6.

Several observations are notable: For example, double hybrids such as B2PLYP [138] perform much better than their high HF exchange fractions would suggest,

because the exact exchange integrals are compensated by explicit pure non-exchange correlation terms via second-order perturbation theory [36, 94]. Also, the optimized exchange functional in the form of, e.g., OPBE [139, 140] or OLYP [141, 142], which does not include exact HF exchange, performs much better and more like a hybrid functional than other GGAs [132, 143]. The O exchange functional has been estimated to have an effect that corresponds to ~15% HF exchange [94]. The accuracy of OPBE supports previous findings by Swart [143, 144]. The O exchange functional was made from B88 by parameterization toward HF unrestricted energies of atoms of the first and second periods, and thus, this parameterization by design includes HF-like energetics. It is very interesting that re-parametrization toward HF energies or, as analyzed by Swart et al. [132] a leading s^4 term in the exchange functional, can cause a GGA non-hybrid exchange functional to behave similarly to a hybrid with 15% HF exchange because it tells us that HF exchange is not a "universal" feature by itself, but a pragmatic solution to a major problem of accuracy [127].

4.2 The Role of the Correlation Functional

Inspection of the original paper by Paulsen et al. [34] reveals that BLYP has the same ~17 kJ/mol smaller bias toward LS than PW91 for two distinct systems. This consistent difference could be coincidental, and even if not, it could be due to many features of the two functionals. Systematic comparison of functional types such as, e.g., BLYP versus BP86 (which use the same exchange functional) shows that the correlation functional, perhaps surprisingly, also contributes systematically to the spin-state balance [132]. Thus, for example, whereas BP86 and PBE give very similar results for SCO energetics and can be considered to have the same spin-state balance, the bias toward LS is reduced by typically 10–15 kJ/mol when using BLYP, and this effect is thus explicitly due to the LYP correlation functional [36].

It is interesting here to comment on the analogy between the performance of DFT applied to SCO and to the modeling of chemical bond strengths. The dissociation energy of a chemical bond is arguably the most fundamental energy of chemistry, as most chemical processes involve breaking and forming bonds with a net effect resembling the involved BDEs. It has been shown many years ago that HF exchange weakens the BDE of bonds, and correspondingly, that the LYP functional also lowers bond energies relative to other correlation functionals [145]. This has been seen repeatedly and is true for bonds involving strictly main-group elements [146] as well as bonds involving transition metals [98, 147]. Thus, the experience with modeling chemical bond strengths and spin-state energetics is intriguingly similar. The reason for this similarity has been proposed [28] to be due to HF exchange generally favoring the looser electron densities and higher spin quantum numbers reminiscent of both the dissociated states upon bond breaking and the high-spin electronic state.

Finally, it is relevant to mention the recent observation by Kulik and coworkers that also the additionally included gradient terms of the metafunctional, as shown for the TPSS functional, contribute to the spin-state balance [52, 148].

4.3 The Use of Quantum-Chemical Benchmarks and the Post-HF Bias

Two very important requirements for further progress in the accurate description of spin states is the use of adequate and reliable benchmark data either from high-level quantum-chemical computations or experimental data, and the proper account of systematic corrections to ensure that the actual property calculated corresponds to the experimental observable. For many SCO systems, the ΔH_{SCO} is in fact available as recently compiled in the SCOFE30 database [36]; these enthalpies can be accurately computed by DFT once ZPE, dispersion, relativistic, and solvent effects are accounted for.

However, more generally, one has to invoke adequate high-level quantum-mechanical benchmarks. One such type of calculation is CCSD(T); another is CASPT2; and a third is diffusion quantum Monte Carlo techniques (DMC). One of the main worries of these benchmarks is that they depend on a single HF reference which includes *all* of the exact exchange energy in a one-determinant basis but *none* of the compensating correlation energy. Whereas this is probably not a problem for the LS state, for the HS state, this single-determinant reference is heavily influenced by the impact of exact HF exchange and the orbitals and electron density must reflect this. A valid question is thus whether the correlated method is truly capable of bringing this overly spin-polarized reference state into complete spin balance by affording most of the compensating correlation energy.

Knowing the HS–LS biases of these benchmark methods is obviously extremely important in order to avoid false conclusions on the performance of functionals versus such a method. Notably, CASPT2 is biased toward configuration state functions with more exchange integrals (i.e., higher spin states), as they have favorable interactions with the HF reference. A modified shifted reference state was introduced into CASPT2 in 2004 [149] but a bias toward HS remained thereafter as shown from a low-lying triplet in the first CASPT2 study of O_2-binding to heme [150] or from the study of other hemes [135]; this bias can be partly remedied by using CC computation of the 3s3p correlation effects in combination with CASPT2 [151].

The CASPT2 example illustrates well a principle that may be a priori true but depends in practice on the implemented correlation method: *A single-reference post-HF method that is not perfectly correlated (i.e., is not full-CI) will not compensate completely the HF exchange of the reference state and will thus carry some bias toward this state*. Due to this "post-HF-bias", such methods will tend to favor HS too much and underbind metal–ligand bonds where more exchange integrals are presented for the dissociated states than for the bound state. A bias with this type of effect was in fact reported in the original paper on the shifted CASPT2 zeroth-order Hamiltonian [149].

The simple mononuclear nitrogen-donor octahedral complex, $[Fe(NH_3)_6]^{2+}$, is ideally suited for comparing method performance as most methods can be applied to this small system [152]. For this system with adequately optimized HS and LS geometries, the adiabatic energy difference for B3LYP is roughly 60 kJ/mol in favor

of HS; this has been shown in multiple studies [52, 143, 153]. From Swart's study, OPBE gives ~80 kJ/mol in favor of HS [143]. Notably, OPBE is known to do well for SCO systems also from the same study [143], and confirmed by us [94]. Thus, one cannot expect the 80 kJ/mol estimate for the relaxed ΔH_{SCO} to be in much error, even when correcting for the systematic dispersion, relativistic, and ZPE effects described above. This value of ~80 kJ/mol is quite similar to the CASPT2 value obtained by Pierloot and Vancoille [152]. From all of these studies, it thus emerges that B3LYP at 60 kJ/mol has an error probably not larger than ~20 kJ/mol for $[Fe(NH_3)_6]^{2+}$.

In stark contrast to these findings is a new benchmark using diffusion Monte Carlo (DMC) based on HF nodal surfaces, which suggests that B3LYP favors LS too much by more than 60 kJ/mol for $[Fe(NH_3)_6]^{2+}$, and TPPSh by almost 100 kJ/mol [153]. DMC in that study suggests that HS is 120 kJ/mol below LS, which seems too much and is 40 kJ/mol more in favor of HS than CASPT2. Similar surprising results with DMC can also be deduced by comparison of $Fe(NCH)_6]^{2+}$ of the new study [153] to the study by Lawson Daku et al. [154] and Kepenekian et al. [155].

One explanation could be that DMC applied to spin-state energetics is very sensitive to the use of the HF nodes for the highly spin-polarized HS state, but this remains to be further investigated. If true, it again illustrates a post-HF bias but this time via the applied fixed node used in DMC. This suspicion is enhanced by a study [156] that investigated the use of different orbitals for the Slater−Jastrow trial wave function with DMC: CASSCF and HF orbitals give similar results and much higher absolute energies by 0.01 a.u. for the HS state and 0.03 a.u. for the LS state than the DFT Kohn–Sham orbitals, showing that the latter orbitals become better correlated during the full computation, as expected from the considerations above (i.e., the removal of the initial HF bias is very difficult). Confirming the suspicion further, the difference amounts to 0.02 a.u. in the computed HS–LS gap, or ~50 kJ/mol, very similar to the hypothesized error in DMC(HF) that can be deduced from the work discussed above [153].

This discussion illustrates (1) the effect of correlation on DMC using DFT rather than HF orbitals for the fixed node approximation, (2) that any quantum-mechanical method that starts from the HF picture will keep some bias toward this state unless fully correlated, which is in practice very hard; and (3) that extreme care should be applied when using supposedly high-level quantum-chemical methods as direct benchmark, rather than experimental data. CASPT2, rather than CCSD(T) which cannot describe non-dynamic correlation as well, is arguably the current "golden standard" of computational spin crossover and may stay so as the use of larger more appropriate active spaces and basis sets become computationally tractable.

4.4 Toward Spin-State-Balanced Density Functionals

The goal of current efforts in theoretical chemistry is to achieve a state where theory becomes truly predictive and thus, accurate enough to explain and design new systems of interest. For DFT, this would mean that a functional can be applied to chemistry

broadly, and to SCO specifically, with predictive accuracy, making the functional "universal" [157–159]. The discussion above suggests that we must continue to improve the quality of density functionals, which will ultimately be used for predicting SCO behavior in larger systems and in batches of many systems, where other quantum-mechanical methods are too computationally slow. However, we should also carefully understand the biases in the quantum-mechanical benchmark methods themselves. Finally, in order to ensure that this process works, we should use the experimental data available for smaller systems where several quantum-chemical methods can be applied.

As has been widely discussed in the literature, different density functionals produce very different HS–LS gaps [28, 30, 36, 49, 52, 61, 64, 89, 118, 129, 132, 143, 160–163]. From these many studies, some consensus is, however, starting to emerge. In this author's humble view, functionals emerging as accurate for SCO include B3LYP* [61] (B3LYP [127, 128, 142] with 15% HF exchange), TPSSh [62, 164] (a meta hybrid with 10% HF exchange), and the double-hybrid B2PLYP [91]. Among GGA functionals, OLYP and OPBE are promising [94, 143]; it uses Handy and Cohen's optimized exchange [139, 141] which favors HS more than other non-hybrid GGA exchange functionals. If combined with LYP [142, 165] it gives even more HS stabilization because LYP is a HS-favoring correlation functional compared to, e.g., PBE, PW91, and P86 [36]. Particularly, encouraging is also the SSB functional which switches between PBE and OPBE [144], utilizing the high accuracy of the O exchange functional for spin-state energetics.

Even within iron SCO, which would supposedly be considered one type of systems for one type of purpose, there are system dependencies in method performance relating to oxidation state, i.e., even for the subset of iron SCO, there is no "universal" functional. It turns out that typical density functionals produce different errors in the spin-state balance for Fe(III) and Fe(II) SCO systems. Thus, for example, B3LYP* is not equally accurate for Fe(III) and Fe(II) systems, and in fact tends to produce too much high spin in Fe(II) systems and too much LS in Fe(III) systems [36]. Hybrid functionals tend to not only favor HS as explained above but also favor HS too much in Fe(II) compared to Fe(III), which has been called the "Fe(II)–Fe(III) bias" of DFT and which readily grows to 20 kJ/mol [94].

One of the more promising, recent avenues is the use of range-separated hybrids to study SCO processes, because these functionals can have several other advantages such as a small self-interaction error and more accurate transition-state energetics. One example of such a range-separated hybrid functional for use in SCO is CAMB3LYP [166]. This functional works surprisingly well by itself, but the 2018-customized versions with slightly less HF exchange (15–17%) are even more accurate [94]. Another example, also from 2018, is the optimally tuned range-separated hybrid (OT-RSH) studied by Prokopiou and Kronik [167], who also found that the short-range HF percentage is the most important parameter for achieving spin-state balance. Thus, for the broader study of transition metal catalysis where transition states are involved of variable spin states, the CAMB3LYP functional is probably among the best currently available, although this remains to be tested by additional benchmark studies.

Many of the catalytic processes that are of fundamental and technological interest involve changes in the spin states. The widely used RPBE functional [168] has a substantially better spin-state balance [94] than the original PBE functional [140] from which it was made, because it is less biased toward LS; this tendency as usual agrees well with the reduced over-binding tendency of RPBE, since HS bias and under-binding goes together [28].

5 Conclusions

This chapter has outlined the basic machinery of thermal SCO in single molecules with a particular focus on the achievements in modeling this process using DFT. The contribution of dispersion forces already in a single molecule undergoing SCO has been discussed; the generic dispersion effect on SCO arising from the first coordination sphere expansion favors the LS state by typical 10 kJ/mol; this generic dispersion term is supplemented by additional contributions from the type and bulkiness of the ligands that can favor either LS or HS. There is also a generic relativistic SCO effect with a surprisingly large contribution to the spin-state balance, typically also 10 kJ/mol in favor of LS but much less variable because the relativistic contribution is dominated by the metal ion and not the different ligands of SCO systems. Considering that typical SCO energies are of the order of 10–20 kJ/mol in favor of LS, these two effects combined favor LS more than the total energy gap. Thus, any conclusion on the accuracy of a theoretical method compared to the "observed ground-state spin" or the experimental enthalpy of SCO should consider these terms. Put another way, a functional without these two terms that gives 20 kJ/mol too much HS compared to experimental ΔH_{SCO} is excellent. If the calculation is compared to observed ground states, which reflect free energies, then one cannot ignore vibrational entropy, which largely determines the spin transition and SCO process. This entropy can be estimated decently but not very precisely from frequency analysis using standard quantum-chemical programs and is less sensitive to DFT functional used but more sensitive to the intermolecular interactions and explicit solvent effects not generally accounted for in current theoretical models of DFT. Once we master the ability to predict quantitatively the single-molecule SCO energetics, which requires an accuracy of about 10 kJ/mol, we can hope to continue to these challenges of real systems in condense states in the near future.

References

1. Halcrow MA (2013) Spin-crossover materials: properties and applications. Wiley
2. Gütlich P, Goodwin HA (2004) Spin crossover—an overall perspective. In: Spin crossover in transition metal compounds I. Springer, pp 1–47
3. Létard J-F, Guionneau P, Goux-Capes L (2004) Towards spin crossover applications. Spin Crossover Transit Met Compd III 1–19

4. Brooker S (2015) Spin crossover with thermal hysteresis: practicalities and lessons learnt. Chem Soc Rev 44:2880–2892
5. Gütlich P, Garcia Y, Goodwin HA (2000) Spin crossover phenomena in Fe(II) complexes. Chem Soc Rev 29:419–427
6. Harding DJ, Harding P, Phonsri W (2016) Spin crossover in iron (III) complexes. Coord Chem Rev 313:38–61
7. Kumar KS, Ruben M (2017) Emerging trends in spin crossover (SCO) based functional materials and devices. Coord Chem Rev 346:176–205
8. Guionneau P (2014) Crystallography and spin-crossover. A view of breathing materials. Dalt Trans 43:382–393
9. Ruiz E (2014) Charge transport properties of spin crossover systems. Phys Chem Chem Phys 16:14–22
10. Cambi L, Szegö L (1931) Über die magnetische Susceptibilität der komplexen Verbindungen. Berichte der Dtsch Chem Gesellschaft A B Ser 64:2591–2598
11. Šalitroš I, Madhu NT, Boča R, Pavlik J, Ruben M (2009) Room-temperature spin-transition iron compounds. Chem Mon 140:695–733
12. Kepp KP (2017) Heme: from quantum spin crossover to oxygen manager of life. Coord Chem Rev 344:363–374
13. Scheidt WR, Reed CA (1981) Spin-state/stereochemical relationships in iron porphyrins: implications for the hemoproteins. Chem Rev 81:543–555
14. Jensen KP, Ryde U (2004) How O_2 binds to heme: reasons for rapid binding and spin inversion. J Biol Chem 279:14561–14569
15. Gaspar AB, Muñoz MC, Real JA (2006) Dinuclear iron (II) spin crossover compounds: singular molecular materials for electronics. J Mater Chem 16:2522–2533
16. Bousseksou A, Molnár G, Demont P, Menegotto J (2003) Observation of a thermal hysteresis loop in the dielectric constant of spin crossover complexes: towards molecular memory devices. J Mater Chem 13:2069–2071
17. Miyamachi T, Gruber M, Davesne V, Bowen M, Boukari S, Joly L, Scheurer F, Rogez G, Yamada TK, Ohresser P (2012) Robust spin crossover and memristance across a single molecule. Nat Commun 3:938
18. Linares J, Codjovi E, Garcia Y (2012) Pressure and temperature spin crossover sensors with optical detection. Sensors 12:4479–4492
19. Salmon L, Molnár G, Zitouni D, Quintero C, Bergaud C, Micheau J-C, Bousseksou A (2010) A novel approach for fluorescent thermometry and thermal imaging purposes using spin crossover nanoparticles. J Mater Chem 20:5499–5503
20. Bartual-Murgui C, Akou A, Thibault C, Molnár G, Vieu C, Salmon L, Bousseksou A (2015) Spin-crossover metal–organic frameworks: promising materials for designing gas sensors. J Mater Chem C 3:1277–1285
21. Manrique-Juarez MD, Mathieu F, Shalabaeva V, Cacheux J, Rat S, Nicu L, Leïchlé T, Salmon L, Molnár G, Bousseksou A (2017) A bistable microelectromechanical system actuated by spin-crossover molecules. Angew Chem 129:8186–8190
22. Shepherd HJ, Il'ya A, Quintero CM, Tricard S, Salmon L, Molnár G, Bousseksou A (2013) Molecular actuators driven by cooperative spin-state switching. Nat Commun 4:2607
23. Harvey JN, Poli R, Smith KM (2003) Understanding the reactivity of transition metal complexes involving multiple spin states. Coord Chem Rev 238:347–361
24. Sorai M, Nakano M, Miyazaki Y (2006) Calorimetric investigation of phase transitions occurring in molecule-based magnets. Chem Rev 106:976–1031
25. Molnár G, Salmon L, Nicolazzi W, Terki F, Bousseksou A (2014) Emerging properties and applications of spin crossover nanomaterials. J Mater Chem C 2:1360–1366
26. Liu T, Zheng H, Kang S, Shiota Y, Hayami S, Mito M, Sato O, Yoshizawa K, Kanegawa S, Duan C (2013) A light-induced spin crossover actuated single-chain magnet. Nat. Commun. 4:2826
27. Cirera J, Ruiz E (2015) Theoretical modeling of two-step spin-crossover transitions in Fe^{II} dinuclear systems. J Mater Chem C 3:7954–7961

28. Kepp KP (2013) Consistent descriptions of metal–ligand bonds and spin-crossover in inorganic chemistry. Coord Chem Rev 257:196–209
29. Toftlund H (2001) Spin equilibrium in solutions. Chem Mon 132:1269–1277
30. Paulsen H, Schünemann V, Wolny JA (2013) Progress in electronic structure calculations on spin-crossover complexes. Eur J Inorg Chem 2013:628–641
31. Saito Y, Takemoto J, Hutchinson B, Nakamoto K (1972) Infrared studies of coordination compounds containing low-oxidation-state metals. I. Tris (2,2′-bipyridine) and tris (1,10-phenanthroline) complexes. Inorg Chem 11:2003–2011
32. Sorai M, Seki S (1974) Phonon coupled cooperative low-spin $^1A_1$ high-spin $^5T_2$ transition in $[Fe(phen)_2(NCS)_2]$ and $[Fe(phen)_2(NCSe)_2]$ crystals. J Phys Chem Solids 35:555–570
33. Kershaw Cook LJ, Kulmaczewski R, Mohammed R, Dudley S, Barrett SA, Little MA, Deeth RJ, Halcrow MA (2016) A unified treatment of the relationship between ligand substituents and spin state in a family of iron (II) complexes. Angew Chem Int Ed 55:4327–4331
34. Paulsen H, Duelund L, Winkler H, Toftlund H, Trautwein AX (2001) Free energy of spin-crossover complexes calculated with density functional methods. Inorg Chem 40:2201–2203
35. Kulshreshtha SK, Sasikala R, König E (1986) Calorimetric investigations of the low-spin ($^1A_1$) $\rightleftarrows$ high-spin ($^5T_2$) transition in solid dithiocyanatobis(2,2′-BI-2-thiazoline iron(III). Chem Phys Lett 123:215–217
36. Kepp KP (2016) Theoretical study of spin crossover in 30 iron complexes. Inorg Chem 55:2717–2727
37. Homma Y, Ishida T (2018) A new $S = 0 \rightleftarrows S = 2$ "Spin-crossover" scenario found in a Nickel (II) Bis (nitroxide) system. Chem Mater 30:1835–1838
38. Shimura Y, Tsuchida R (1956) Absorption spectra of Co(III) complexes. II. Redetermination of the spectrochemical series. Bull Chem Soc Jpn 29:311–316
39. Jørgensen CK (1959) Electron transfer spectra of hexahalide complexes. Mol Phys 2:309–332
40. Baker WA Jr, Bobonich HM (1964) Magnetic properties of some high-spin complexes of iron (II). Inorg Chem 3:1184–1188
41. König E, Madeja K (1966) Unusual magnetic behaviour of some iron (II)–bis-(1, 10-phenanthroline) complexes. Chem Commun 61–62
42. Koenig E, Madeja K (1967) $^5T_2$-$^1A_1$ Equilibriums in some iron (II)-bis (1, 10-phenanthroline) complexes. Inorg Chem 6:48–55
43. König E, Madeja K (1967) Infra-red spectra at the $^5T_2$-$^1A_1$ cross-over in iron (II) complexes. Spectrochim Acta Part A Mol Spectrosc 23:45–54
44. Stoufer RC, Busch DH, Hadley WB (1961) Unusual magnetic properties of some six-coordinate cobalt(II) complexes—electronic isomers. J Am Chem Soc 83:3732–3734
45. Pauling L (1932) The nature of the chemical bond. III. The transition from one extreme bond type to another. J Am Chem Soc 54:988–1003
46. Tsuchida R (1938) Absorption spectra of co-ordination compounds. I. Bull Chem Soc Jpn 13:388–400
47. Fajans K (1923) Struktur und Deformation der Elektronenhüllen in ihrer Bedeutung für die chemischen und optischen Eigenschaften anorganischer Verbindungen. Naturwissenschaften 11:165–172
48. König E (1968) Some aspects of the chemistry of bis (2,2′-dipyridyl) and bis (1,10-phenanthroline) complexes of iron (II). Coord Chem Rev 3:471–495
49. Houghton BJ, Deeth RJ (2014) Spin-state energetics of FeII complexes-the continuing voyage through the density functional minefield. Eur J Inorg Chem 2014:4573–4580
50. Deeth RJ, Anastasi AE, Wilcockson MJ (2010) An in silico design tool for Fe(II) spin crossover and light-induced excited spin state-trapped complexes. J Am Chem Soc 132:6876–6877
51. Deeth RJ, Halcrow MA, Kershaw Cook LJ, Raithby PR (2018) Ab initio ligand field molecular mechanics and the nature of metal-ligand π-bonding in Fe(II) 2,6-di(pyrazol-1-yl)pyridine spin crossover complexes. Chem Eur J 24:5204–5212
52. Mortensen SR, Kepp KP (2015) Spin propensities of octahedral complexes from density functional theory. J Phys Chem A 119:4041–4050

53. Takemoto JH, Hutchinson B (1973) Low-frequency infrared spectra of complexes which exhibit magnetic crossover. I. Iron(II) complexes of 1,10-phenanthroline and 2,2′-bipyridine. Inorg Chem 12:705–708
54. Kepp KP (2011) The ground states of iron(III) porphines: Role of entropy-enthalpy compensation, Fermi correlation, dispersion, and zero-point energies. J Inorg Biochem 105:1286–1292
55. Ashley DC, Jakubikova E (2017) Ironing out the photochemical and spin-crossover behavior of Fe (II) coordination compounds with computational chemistry. Coord Chem, Rev
56. Phonsri W, Davies CG, Jameson GNL, Moubaraki B, Ward JS, Kruger PE, Chastanet G, Murray KS (2017) Symmetry breaking above room temperature in an Fe (ii) spin crossover complex with an N4O2 donor set. Chem Commun 53:1374–1377
57. Yamasaki M, Ishida T (2015) First Iron(II) spin-crossover complex with an N5S coordination sphere. Chem Lett 44:920–921
58. Phan H, Hrudka JJ, Igimbayeva D, Lawson Daku LM, Shatruk M (2017) A simple approach for predicting the spin state of homoleptic Fe(II) tris-diimine complexes. J Am Chem Soc 139:6437–6447
59. Scott HS, Staniland RW, Kruger PE (2018) Spin crossover in homoleptic Fe(II) imidazolylimine complexes. Coord Chem Rev 362:24–43
60. Reiher M, Salomon O, Hess BA (2001) Reparameterization of hybrid functionals based on energy differences of states of different multiplicity. Theor Chem Acc 107:48–55
61. Salomon O, Reiher M, Hess BA (2002) Assertion and validation of the performance of the B3LYP* functional for the first transition metal row and the G2 test set. J Chem Phys 117:4729–4737
62. Tao J, Perdew JP, Staroverov VN, Scuseria GE (2003) Climbing the density functional ladder: nonempirical meta generalized gradient approximation designed for molecules and solids. Phys Rev Lett 91:146401
63. Jensen KP (2008) Bioinorganic chemistry modeled with the TPSSh density functional. Inorg Chem 47:10357–10365
64. Jensen KP, Cirera J (2009) Accurate computed enthalpies of spin crossover in iron and cobalt complexes. J Phys Chem A 113:10033–10039
65. Gütlich P, McGarvey BR, Kläui W (1980) Temperature-dependent $^5T_2$ (O_h) $\rightleftharpoons$ $^1A_1$ (O_h) spin equilibrium in a six-coordinate cobalt (III) complex. Investigation by phosphorus-31 NMR in solution. Inorg Chem 19:3704–3706
66. Kläui W (1980) High spin-low spin equilibrium in six-coordinate cobalt(III) complexes. Inorganica Chim Acta 40:X22–X23
67. Kläui W, Eberspach W, Guetlich P (1987) Spin-crossover cobalt(III) complexes: steric and electronic control of spin state. Inorg Chem 26:3977–3982
68. Chen J-M, Chin Y-Y, Valldor M, Hu Z, Lee J-M, Haw S-C, Hiraoka N, Ishii H, Pao C-W, Tsuei K-D (2014) A complete high-to-low spin state transition of trivalent cobalt ion in octahedral symmetry in $SrCo_{0.5}Ru_{0.5}O_{3-\delta}$. J Am Chem Soc 136:1514–1519
69. Stauber JM, Zhang S, Gvozdik N, Jiang Y, Avena L, Stevenson KJ, Cummins CC (2018) Cobalt and vanadium trimetaphosphate polyanions: synthesis, characterization, and electrochemical evaluation for non-aqueous redox-flow battery applications. J Am Chem Soc 140:538–541
70. Hayami S, Nakaya M, Ohmagari H, Alao AS, Nakamura M, Ohtani R, Yamaguchi R, Kuroda-Sowa T, Clegg JK (2015) Spin-crossover behaviors in solvated cobalt (II) compounds. Dalt Trans 44:9345–9348
71. Hayami S, Komatsu Y, Shimizu T, Kamihata H, Lee YH (2011) Spin-crossover in cobalt (II) compounds containing terpyridine and its derivatives. Coord Chem Rev 255:1981–1990
72. Krivokapic I, Zerara M, Daku ML, Vargas A, Enachescu C, Ambrus C, Tregenna-Piggott P, Amstutz N, Krausz E, Hauser A (2007) Spin-crossover in cobalt (II) imine complexes. Coord Chem Rev 251:364–378
73. Guo Y, Yang X-L, Wei R-J, Zheng L-S, Tao J (2015) Spin transition and structural transformation in a mononuclear Cobalt(II) complex. Inorg Chem 54:7670–7672
74. Radon M, Drabik G (2018) Spin states and other ligand–field states of aqua complexes revisited with multireference ab initio calculations including solvation effects. J Chem Theory Comput

75. Nielsen MT, Moltved KA, Kepp KP (2018) Electron transfer of hydrated transition-metal ions and the electronic state of Co^{3+}(aq). Inorg Chem 57:7914–7924
76. Johnson DA, Sharpe AG (1964) Reactions of cobalt(III) compounds: magnitude of Cobalt(III)/Cobalt(II) standard potential in aqueous solution. J Chem Soc 3490–3492
77. Winkler JR, Rice SF, Gray HB (1981) On the role of the high-spin state in the water exchange reaction of Hexaaquocobalt(III). Comments Inorg Chem 1:47–51
78. Navon G (1981) A search for the thermally populated high-spin excited state of hexaaquocobalt(3+) by coblt NMR. J Phys Chem 85:3547–3549
79. Habib HS, Hunt JP (1966) Electron-transfer reactions between aqueous cobaltous and cobaltic ions. J Am Chem Soc 88:1668–1671
80. Chou M, Creutz C, Sutin N (1977) Rate constants and activation parameters for outer-sphere electron-transfer reactions and comparisons with the predictions of Marcus theory. J Am Chem Soc 99:5615–5623
81. Shatruk M, Phan H, Chrisostomo BA, Suleimenova A (2015) Symmetry-breaking structural phase transitions in spin crossover complexes. Coord Chem Rev 289–290:62–73
82. Ni Z-P, Liu J-L, Hoque MN, Liu W, Li J-Y, Chen Y-C, Tong M-L (2017) Recent advances in guest effects on spin-crossover behavior in Hofmann-type metal-organic frameworks. Coord Chem Rev 335:28–43
83. Halder GJ, Kepert CJ, Moubaraki B, Murray KS, Cashion JD (2002) Guest-dependent spin crossover in a nanoporous molecular framework material. Science (80–) 298:1762–1765
84. Struch N, Bannwarth C, Ronson TK, Lorenz Y, Mienert B, Wagner N, Engeser M, Bill E, Puttreddy R, Rissanen K (2017) An octanuclear metallosupramolecular cage designed to exhibit spin-crossover behavior. Angew Chem Int Ed 56:4930–4935
85. Kumar KS, Studniarek M, Heinrich B, Arabski J, Schmerber G, Bowen M, Boukari S, Beaurepaire E, Dreiser J, Ruben M (2018) Engineering on-surface spin crossover: spin-state switching in a self-assembled film of vacuum-sublimable functional molecule. Adv Mater 30:1705416
86. Zhang L, Kepp KP, Ulstrup J, Zhang J (2018) Redox potentials and electronic states of iron porphyrin IX adsorbed on single crystal gold electrode surfaces. Langmuir 34:3610–3618
87. Kepenekian M, Le Guennic B, Robert V (2009) Primary role of the electrostatic contributions in a rational growth of hysteresis loop in spin-crossover Fe (II) complexes. J Am Chem Soc 131:11498–11502
88. Kahn O, Martinez CJ (1998) Spin-transition polymers: from molecular materials toward memory devices. Science 279:44–48
89. Cirera J, Ruiz E (2016) Theoretical modeling of the ligand-tuning effect over the transition temperature in four-coordinated FeII molecules. Inorg Chem 55:1657–1663
90. Tailleur E, Marchivie M, Daro N, Chastanet G, Guionneau P (2017) Thermal spin-crossover with a large hysteresis spanning room temperature in a mononuclear complex. Chem Commun 53:4763–4766
91. Grimme S, Antony J, Ehrlich S, Krieg H (2010) A consistent and accurate ab initio parametrization of density functional dispersion correction (DFT-D) for the 94 elements H-Pu. J Chem Phys 132:154104
92. Bučko T, Hafner J, Lebègue S, Ángyán JG (2012) Spin crossover transition of $Fe(phen)_2(NCS)_2$: periodic dispersion-corrected density-functional study. Phys Chem Chem Phys 14:5389–5396
93. Timken MD, Wilson SR, Hendrickson DN (1985) Dynamics of spin-state interconversion and cooperativity for ferric spin-crossover complexes in the solid state. 4. Pyruvic acid thiosemicarbazone complex. Inorg Chem 24:3450–3457
94. Siig OS, Kepp KP (2018) Iron (II) and Iron (III) spin crossover: toward an optimal density functional. J Phys Chem A 122:4208–4217
95. Kepp KP, Dasmeh P (2013) Effect of distal interactions on O_2 binding to heme. J Phys Chem B 117:3755–3770
96. Kepp KP (2017) Heme isomers substantially affect heme's electronic structure and function. Phys Chem Chem Phys 19:22355–22362

97. Pyykkö P (2012) Relativistic effects in chemistry: more common than you thought. Annu Rev Phys Chem 63:45–64
98. Jensen KP, Roos BO, Ryde U (2007) Performance of density functionals for first row transition metal systems. J Chem Phys 126:14103
99. Hess BA (1986) Relativistic electronic-structure calculations employing a two-component no-pair formalism with external-field projection operators. Phys Rev A 33:3742
100. Reiher M, Wolf A (2004) Exact decoupling of the Dirac Hamiltonian. I. General theory. J Chem Phys 121:2037–2047
101. Moore CE (1971) Atomic energy levels. Atomic energy levels. United States Department of Commerce & National Bureau of Standards, Washington, DC, pp 56–57
102. Sousa C, Domingo A, de Graaf C (2018) Effect of second-order spin-orbit coupling on the interaction between spin states in spin-crossover systems. Chem Eur J 24:5146–5152
103. de Graaf C, Sousa C (2010) Study of the light-induced spin crossover process of the $[Fe^{II}(bpy)_3]^{2+}$ complex. Chem Eur J 16:4550–4556
104. Paulsen H, Trautwein AX (2004) Density functional theory calculations for spin crossover complexes. In: Spin crossover in transition metal compounds III. Springer, pp 197–219
105. Pyykko P (1988) Relativistic effects in structural chemistry. Chem Rev 88:563–594
106. Nakamoto T, Tan Z-C, Sorai M (2001) Heat capacity of the spin crossover complex $[Fe(2\text{-}pic)_3]Cl_2{\cdot}MeOH$: a spin crossover phenomenon with weak cooperativity in the solid state. Inorg Chem 40:3805–3809
107. Sorai M (2001) Calorimetric investigations of phase transitions occurring in molecule-based materials in which electrons are directly involved. Bull Chem Soc Jpn 74:2223–2253
108. Addison AW, Burman S, Wahlgren CG, Rajan OA, Rowe TM, Sinn E (1987) New iron (II) spin-crossover complexes with heterocyclic amine-derived ligands and STEPS experiments on photogenerated metastable high-spin states. J Chem Soc Dalt Trans 2621–2630
109. Chum HL, Vanin JA, Holanda MID (1982) Tris (2-(aminomethyl) pyridine)iron(II): a new spin-state equilibrium in solution. Inorg Chem 21:1146–1152
110. Létard J-F, Guionneau P, Rabardel L, Howard JAK, Goeta AE, Chasseau D, Kahn O (1998) Structural, magnetic, and photomagnetic studies of a mononuclear iron (II) derivative exhibiting an exceptionally abrupt spin transition. Light-induced thermal hysteresis phenomenon. Inorg Chem 37:4432–4441
111. Strauß B, Linert W, Gutmann V, Jameson RF (1992) Spin-crossover complexes in solution, I. Substitutional lability of $[Fe(bzimpy)_2](ClO_4)_2$. Chem Mon 123:537–546
112. Boča R, Boča M, Dlháň L, Falk K, Fuess H, Haase W, Jaroščiak R, Papánková B, Renz F, Vrbová M, Werner R (2001) Strong cooperativeness in the mononuclear iron(II) derivative exhibiting an abrupt spin transition above 400 K. Inorg Chem 40:3025–3033
113. Nakamoto T, Bhattacharjee A, Sorai M (2004) Cause for unusually large thermal hysteresis of spin crossover in $[Fe(2\text{-}pic)_3]Cl_2{\cdot}$ H2O. Bull Chem Soc Jpn 77:921–932
114. Bartel M, Absmeier A, Jameson GNL, Werner F, Kato K, Takata M, Boca R, Hasegawa M, Mereiter K, Caneschi A (2007) Modification of spin crossover behavior through solvent assisted formation and solvent inclusion in a triply interpenetrating three-dimensional network. Inorg Chem 46:4220–4229
115. Lemercier G, Bousseksou A, Verelst M, Varret F, Tuchagues JP (1995) Dynamic spin-crossover in $[FeII(TRIM)_2]Cl_2$ investigated by Mössbauer spectroscopy and magnetic measurements. J Magn Magn Mater 150:227–230
116. Dose EV, Murphy KMM, Wilson LJ (1976) Synthesis and spin-state studies in solution of γ-substituted tris (β-diketonato) iron(III) complexes and their spin-equilibrium. β-ketoimine analogues derived from triethylenetetramine. Inorg Chem 15:2622–2630
117. Ye S, Neese F (2010) Accurate modeling of spin-state energetics in spin-crossover systems with modern density functional theory. Inorg Chem 49:772–774
118. Conradie J, Ghosh A (2007) DFT calculations on the spin-crossover complex Fe (salen)(NO): a quest for the best functional. J Phys Chem B 111:12621–12624
119. Li Z, Dai J, Shiota Y, Yoshizawa K, Kanegawa S, Sato O (2013) Multi-step spin crossover accompanied by symmetry breaking in an FeIII complex: crystallographic evidence and DFT studies. Chem Eur J 19:12948–12952

120. de Visser SP (2005) What affects the quartet-doublet energy splitting in peroxidase enzymes? J Phys Chem A 109:11050–11057
121. Franzen S (2002) Spin-dependent mechanism for diatomic ligand binding to heme. Proc Natl Acad Sci USA 99:16754–16759
122. Bousseksou A, McGarvey JJ, Varret F, Real JA, Tuchagues J-P, Dennis AC, Boillot ML (2000) Raman spectroscopy of the high-and low-spin states of the spin crossover complex $Fe(phen)_2(NCS)_2$: an initial approach to estimation of vibrational contributions to the associated entropy change. Chem Phys Lett 318:409–416
123. Molnár G, Niel V, Gaspar AB, Real J-A, Zwick A, Bousseksou A, McGarvey JJ (2002) Vibrational spectroscopy of cyanide-bridged, iron (II) spin-crossover coordination polymers: estimation of vibrational contributions to the entropy change associated with the spin transition. J Phys Chem B 106:9701–9707
124. Ronayne KL, Paulsen H, Höfer A, Dennis AC, Wolny JA, Chumakov AI, Schünemann V, Winkler H, Spiering H, Bousseksou A (2006) Vibrational spectrum of the spin crossover complex $[Fe(phen)_2(NCS)_2]$ studied by IR and Raman spectroscopy, nuclear inelastic scattering and DFT calculations. Phys Chem Chem Phys 8:4685–4693
125. Brehm G, Reiher M, Schneider S (2002) Estimation of the vibrational contribution to the entropy change associated with the low-to high-spin transition in $Fe(phen)_2(NCS)_2$ complexes: results obtained by IR and Raman spectroscopy and DFT calculations. J Phys Chem A 106:12024–12034
126. Becke AD (1993) A new mixing of Hartree-Fock and local density-functional theories. J Chem Phys 98:1372–1377
127. Becke AD (1993) Density-functional thermochemistry. III. The role of exact exchange. J Chem Phys 98:5648–5652
128. Stephens PJ, Devlin FJ, Chabalowski CF, Frisch MJ (1994) Ab initio calculation of vibrational absorption and circular dichroism spectra using density functional force fields. J Phys Chem 98:11623–11627
129. Reiher M (2002) Theoretical study of the $Fe(phen)_2(NCS)_2$ spin-crossover complex with reparametrized density functionals. Inorg Chem 41:6928–6935
130. Cirera J, Paesani F (2012) Theoretical prediction of spin-crossover temperatures in ligand-driven light-induced spin change systems. Inorg Chem 51:8194–8201
131. Gani TZH, Kulik HJ (2017) Unifying exchange sensitivity in transition-metal spin-state ordering and catalysis through bond valence metrics. J Chem Theory Comput 13:5443–5457
132. Swart M, Groenhof AR, Ehlers AW, Lammertsma K (2004) Validation of exchange-correlation functionals for spin states of iron complexes. J Phys Chem A 108:5479–5483
133. Harvey JN (2004) DFT computation of relative spin-state energetics of transition metal compounds. In: Principles and applications of density functional theory in inorganic chemistry I. Springer, pp 151–184
134. Ghosh A (2006) Transition metal spin state energetics and noninnocent systems: challenges for DFT in the bioinorganic arena. J Biol Inorg Chem 11:712–724
135. Vancoillie S, Zhao H, Radon M, Pierloot K (2010) Performance of CASPT2 and DFT for relative spin-state energetics of heme models. J Chem Theory Comput 6:576–582
136. Hughes TF, Friesner RA (2011) Correcting systematic errors in DFT spin-splitting energetics for transition metal complexes. J Chem Theory Comput 7:19–32
137. Pinter B, Chankisjijev A, Geerlings P, Harvey JN, De Proft F (2018) Conceptual insights into DFT spin-state energetics of octahedral transition-metal complexes through a density difference analysis. Chem Eur J 24:5281–5292
138. Grimme S (2006) Semiempirical hybrid density functional with perturbative second-order correlation. J Chem Phys 124:34108
139. Cohen AJ, Handy NC (2000) Assessment of exchange correlation functionals. Chem Phys Lett 316:160–166
140. Perdew JP, Burke K, Ernzerhof M (1996) Generalized gradient approximation made simple. Phys Rev Lett 77:3865
141. Handy NC, Cohen AJ (2001) Left-right correlation energy. Mol Phys 99:403–412

142. Lee C, Yang W, Parr RG (1988) Development of the Colle-Salvetti correlation-energy formula into a functional of the electron density. Phys Rev B 37:785–789
143. Swart M (2008) Accurate spin-state energies for iron complexes. J Chem Theory Comput 4:2057–2066
144. Swart M, Solà M, Bickelhaupt FM (2009) A new all-round density functional based on spin states and S_N2 barriers. J Chem Phys 131:94103
145. Jensen K, Ryde U (2003) Theoretical prediction of the Co-C bond strength in cobalamins. J Phys Chem A 155:7539–7545
146. Kepp KP (2017) Trends in strong chemical bonding in C_2, CN, CN^-, CO, N_2, NO, NO^+, and O_2. J Phys Chem A 121:9092–9098
147. Xu X, Zhang W, Tang M, Truhlar DG (2015) Do practical standard coupled cluster calculations agree better than Kohn-Sham calculations with currently available functionals when compared to the best available experimental data for dissociation energies of bonds to 3d transition metals? J Chem Theory Comput 11:2036–2052
148. Ioannidis EI, Kulik HJ (2017) Ligand-field-dependent behavior of meta-GGA exchange in transition-metal complex spin-state ordering. J Phys Chem A 121:874–884
149. Ghigo G, Roos BO, Malmqvist P-Å (2004) A modified definition of the zeroth-order Hamiltonian in multiconfigurational perturbation theory (CASPT2). Chem Phys Lett 396:142–149
150. Jensen KP, Roos B, Ryde U (2005) O_2-binding to heme: electronic structure and spectrum of oxyheme, studied by multiconfigurational methods. J Inorg Biochem 99:45–54
151. Phung QM, Feldt M, Harvey JN, Pierloot K (2018) Toward highly accurate spin state energetics in first-row transition metal complexes: a combined CASPT2/CC approach. J Chem Theory Comput 14:2446–2455
152. Pierloot K, Vancoillie S (2006) Relative energy of the high-($^5T_{2g}$) and low-($^1A_{1g}$) spin states of $[Fe(H_2O)_6]^{2+}$,$[Fe(NH_3)_6]^{2+}$, and $[Fe(bpy)_3]^{2+}$: CASPT2 versus density functional theory. J Chem Phys 125:124303
153. Song S, Kim M-C, Sim E, Benali A, Heinonen O, Burke K (2018) Benchmarks and reliable DFT results for spin gaps of small ligand Fe(II) complexes. J Chem Theory Comput 14:2304–2311
154. Lawson Daku LM, Aquilante F, Robinson TW, Hauser A (2012) Accurate spin-state energetics of transition metal complexes. 1. CCSD(T), CASPT2, and DFT study of $[M(NCH)_6]^{2+}$ (M = Fe, Co). J Chem Theory Comput 8:4216–4231
155. Kepenekian M, Robert V, Le Guennic B, De Graaf C (2009) Energetics of $[Fe(NCH)_6]^{2+}$ via CASPT2 calculations: a spin-crossover perspective. J Comput Chem 30:2327–2333
156. Fumanal M, Wagner LK, Sanvito S, Droghetti A (2016) Diffusion Monte Carlo perspective on the spin-state energetics of $[Fe(NCH)_6]^{2+}$. J Chem Theory Comput 12:4233–4241
157. Peverati R, Truhlar DG (2014) Quest for a universal density functional: the accuracy of density functionals across a broad spectrum of databases in chemistry and physics. Philos Trans R Soc Lond A Math Phys Eng Sci 372:20120476
158. Medvedev MG, Bushmarinov IS, Sun J, Perdew JP, Lyssenko KA (2017) Density functional theory is straying from the path toward the exact functional. Science 355:49–52
159. Kepp KP (2017) Comment on "Density functional theory is straying from the path toward the exact functional". Science 356:496–497
160. Isley WC III, Zarra S, Carlson RK, Bilbeisi RA, Ronson TK, Nitschke JR, Gagliardi L, Cramer CJ (2014) Predicting paramagnetic ^1H NMR chemical shifts and state-energy separations in spin-crossover host–guest systems. Phys Chem Chem Phys 16:10620–10628
161. Ioannidis EI, Kulik HJ (2015) Towards quantifying the role of exact exchange in predictions of transition metal complex properties. J Chem Phys 143:34104
162. Coskun D, Jerome SV, Friesner RA (2016) Evaluation of the performance of the B3LYP, PBE0, and M06 DFT functionals, and DBLOC-corrected versions, in the calculation of redox potentials and spin splittings for transition metal containing systems. J Chem Theory Comput 12:1121–1128
163. Verma P, Varga Z, Klein JEMN, Cramer CJ, Que L, Truhlar DG (2017) Assessment of electronic structure methods for the determination of the ground spin states of Fe(II), Fe(III) and Fe(IV) complexes. Phys Chem Chem Phys 19:13049–13069

164. Perdew JP, Tao J, Staroverov VN, Scuseria GE (2004) Meta-generalized gradient approximation: explanation of a realistic nonempirical density functional. J Chem Phys 120
165. Colle R, Salvetti O (1975) Approximate calculation of the correlation energy for the closed shells. Theor Chim Acta 37:329–334
166. Yanai T, Tew DP, Handy NC (2004) A new hybrid exchange–correlation functional using the Coulomb-attenuating method (CAM-B3LYP). Chem Phys Lett 393:51–57
167. Prokopiou G, Kronik L (2018) Spin-state energetics of Fe complexes from an optimally tuned range-separated hybrid functional. Chem Eur J 24:5173–5182
168. Hammer B, Hansen LB, Nørskov JK (1999) Improved adsorption energetics within density-functional theory using revised Perdew-Burke-Ernzerhof functionals. Phys Rev B 59:7413